Ecological Informatics 90 (2025) 103233

Contents lists available at ScienceDirect

Ecological Informatics

journal homepage: www.elsevier.com/locate/ecolinf

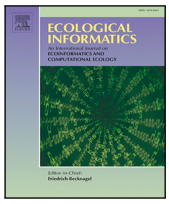

Peatland pixel-level classification via multispectral, multiresolution and multisensor data using convolutional neural network

Luca Zelioli [a], Fahimeh Farahnakian [a,b,*], Maarit Middleton [b], Timo P. Pitkänen [c], Sakari Tuominen [c], Paavo Nevalainen [a], Jonne Pohjankukka [a], Jukka Heikkonen [a]

[a] Department of Computing, University of Turku, Finland
[b] Geological Survey of Finland (GTK), Finland
[c] Natural Resources Institute Finland (Luke), Finland

ARTICLE INFO

Dataset link: https://github.com/MaaTi-project/Peatland-MultiSensor-CNN, https://tupa.gtk.fi/paikkatieto/meta/turvevarojen_tilinpitotiedot.html, https://asiointi.maanmittauslaitos.fi/karttapaikka/tiedostopalvelu?lang=en, https://www.metsakeskus.fi/fi/avoin-metsa-ja-luontotieto/aineistot-paikkatieto-ohjelmille/paikkatieto aineistot, http://kartta.luke.fi/index-en.html

Keywords:
Peatland site type mapping
Multi-sensor fusion
Convolutional neural network
Feature selection
Sliding window
Greenhouse gas inventory
Biodiversity conservation
Remote sensing
Land cover classification

ABSTRACT

High-resolution mapping of boreal peatlands is crucial for greenhouse gas inventories, ecological monitoring, and sustainable land management. However, accurately classifying peatland ecotypes at large scales remains challenging due to the complex phenological changes, dense tree canopies, water table level variations, and the mosaiced structure of vegetation communities typical of these landscapes. To address these challenges, we propose a novel multi-modal convolutional neural network (CNN) architecture designed specifically for pixel-level peatland classification. The motivation behind this research stems from the need for improved accuracy in peatland site type and fertility level mapping, which is vital for effective environmental decision-making. The core strategy of our method involves a late fusion architecture that seamlessly integrates multi-source remote sensing (RS) data, including optical imagery, synthetic aperture radar (SAR), airborne laser scanning (ALS), and multi-source national forest inventory (MS-NFI) datasets. These diverse data sources, characterized by different spatial resolutions, are fused to preserve their spatial integrity, enabling richer feature extraction for classification tasks. Additionally, a sliding-window approach is applied to manage multi-resolution datasets, enhancing pixel-wise classification by preserving spatial and contextual relationships. We evaluated the proposed architecture across three diverse peatland zones in Finland, demonstrating its capability to generalize across varying ecological conditions. Experimental results indicate classification accuracies for peatland site types and fertility levels ranging from 36.6% to 55.0%, highlighting the effectiveness of our approach even with limited labeled training samples. Canopy height models, Sentinel-2 bands, and Sentinel-1 bands emerged as the most influential data sources for accurate classification. Our findings underscore the potential of integrating multi-source RS data with advanced CNN architectures for large-scale peatland mapping. Future work will focus on incorporating LiDAR-derived vegetation structural indices, hyperspectral RS data, and expanding the training dataset to further enhance classification performance.

1. Introduction

Land cover pixel-level classification, i.e. semantic segmentation, is one of the main application areas of remote sensing as it can be used in a wide range of research fields such as urban modeling (Kampffmeyer et al., 2016), agriculture (Liao et al., 2020), change detection (Pouliot et al., 2019), coastal management (Ghobadi et al., 2012) and forest ecology (Korpela et al., 2009). Peatlands cover 3% of the global total land area and half of the Earth's wetlands (Ghobadi et al., 2012). Twelve percent of them are situated in Europe and 57% are boreal peatlands (Programme, 2022-11), such as in Finland, where they cover 30% of the land. They are very important for global climate as they can store enormous amounts of carbon (Finland, 2022). In addition, peatlands act as reservoirs for floodwater retention, habitats for wildlife as well as protected and endangered species, and if artificially drained, are also utilized for forestry and agriculture (Ghobadi et al., 2012; Sugumaran et al., 2004). To maintain existing peatland ecosystems and to inventory greenhouse gas emissions of the drained peatlands, mapping and monitoring of peatland site types, fertility levels, land use and their artificial drainage status are necessary. However, pixel-level classification of complex and heterogeneous land cover types such as peatlands is still a challenging task despite significant improvements in remote sensing (RS) technologies. This is because, in highly fragmented landscapes, many site types are not clearly defined, but they form gradients transforming from one site type to another which, in

* Corresponding author at: Department of Computing, University of Turku, Finland.
E-mail address: fahfar@utu.fi (F. Farahnakian).

https://doi.org/10.1016/j.ecoinf.2025.103233
Received 1 November 2024; Received in revised form 23 May 2025; Accepted 24 May 2025
Available online 30 June 2025

turn, increases the within-class variability and decreases between class separability. In addition, especially in Finland human activities such as transformation of the peatland ecology by artificial forestry drainage has profoundly changed the species structure of understorey layer and tree canopy. Thus, many site type classes have similar characteristics in commonly used optical (Dechka et al., 2002), microwave (Henderson and Lewis, 2008) and Airborne Laser Scanning (ALS) (Korpela et al., 2009) datasets. Thus, boreal peatland classification with RS and machine learning (ML) is found cumbersome at site type level (Räsänen and Virtanen, 2019) whereas higher hierarchical level classifications into wetland-heatland, biotope and habitat levels are successful with RS (Chasmer et al., 2020).

Several studies have recently shown the potential of ML methods for boreal peatland classification including random forest (RF) (Millard and Richardson, 2015; Bourgeau-Chavez et al., 2016; Amoakoh et al., 2021), support vector machine (SVM) (Merchant et al., 2017; Middleton et al., 2012) and decision tree (Chasmer et al., 2020). In this paper (Middleton et al., 2023), we also evaluated k-nearest neighbor (Knn), RF, logistic regression (LR), and multi-layer perceptrons (MLP) for peatland classification based on multivariate analysis of RS data, containing above mentioned satellite and airborne RS and geospatial data sources. However, these methods require feature engineering to extract these information manually. Recent advances in deep learning for remote sensing have introduced powerful models for pixel-level classification and multi-source data fusion. Among these, ResMorCNN (Esmaeili et al., 2023) leverages residual-injection morphological features combined with 3D CNN layers to enhance hyperspectral image classification. This architecture effectively captures spatial–spectral correlations, leading to improved feature representation. To address the challenges of high-dimensional RS data, CNNeGA (Mohammad et al., 2023) proposes a CNN-embedded genetic algorithm for optimal band selection, reducing redundancy while preserving key spectral information. This method has proven effective for hyperspectral imagery where dimensionality reduction is critical. For applications involving multimodal data, HypsLiDNet (Farmonov et al., 2024) introduces a 3D-2D CNN model that employs spatial–spectral morphological attention for crop classification. This approach integrates DESIS and LiDAR data, achieving high classification accuracy across different vegetation types. Further extending multi-modal fusion capabilities, Sharifi et al. (2025) present a deep learning model that effectively integrates hyperspectral and LiDAR data for land cover classification. This work demonstrates the potential of multi-modal deep learning to enhance classification accuracy by exploiting complementary spatial and spectral features. Similarly, the work by Sharifi and Safari (2025) explores advanced fusion techniques, leveraging deep learning to improve land cover mapping accuracy through joint feature extraction from hyperspectral and LiDAR datasets. In light of these developments, our proposed multimodal CNN architecture builds upon these state-of-the-art models by integrating optical imagery, SAR, ALS, and forest inventory datasets. Unlike previous studies, our approach maintains the spatial resolution of each data source and optimizes feature selection through a modified SFS method, specifically addressing the challenges of peatland site type and fertility level classification. CNN-based fusion approaches (Farahnakian and Heikkonen, 2020; Fahimeh and Jukka, 2020; Rudner et al., 2019) show that the performance of CNN can be improved in RS applications by fusing data from various sensors. Although, high dimension of spectral bands can cause a massive learnable kernels for CNN, which is hard to train while increasing computational complexities. For this reason, in this paper (Farahnakian et al., 2023a), we first used two open-source satellite input image sources, Sentinel-1 SAR and optical Sentinel-2, for peatland fertility classification. In addition, we investigated how the fusion level effects the results when we combine these two input data. Early and late fusion architectures were considered. We concluded that late fusion is more effective for combining features as it can merge various features or representations of data at a later stage in the classification process, after these features have been independently processed or extracted.

The existing CNN-based methods for vegetation RS have been reported mostly in three contexts: agriculture, forestry and conservation. In Amoakoh et al. (2021), the random forest algorithm was used for tropical peatland classification using multisensor satellite imagery in Greater Amanzule, Ghana. Another work conducted in Erudel et al. (2017) classifies 13 peatland vegetation types using supervised algorithms such RF, SVM and LR. These traditional classification algorithms have advantages and disadvantages in terms of accuracy, data type used and the ease of analysis. In peatland or wetland classifications, e.g. in Pouliot et al. (2019), a CNN model is proposed for mapping of wetland types at regional scales with multispectral Landsat and polarimetric RADARSAT-2 data. The wetland types in this study includes bog, fen, marsh, and swamp. In Rezaee et al. (2018a), a pretrained AlexNet (Krizhevsky et al., 2012a) is used for weatland mapping. Their results show that CNN was superior to RF for complex wetland mapping. In de Bem et al. (2020), the authors used three CNN models (SharpMask, U-Net, and ResUnet) to detect the changes of deforestation in the Amazon using stacked pairs of Landsat imagery. They also compared the proposed CNNs with two ML algorithms, RF and MLP, and showed that the CNN models provided better performance than the other ML algorithms. In Mohammadimanesh et al. (2019), SAR images have been used for boreal wetland classification in Canada. The features extracted from SAR imagery were passed to the RF algorithms to classify sites into 8 different classes. Training DL-based algorithms require a higher number of samples, which is costly and time-consuming. In the study (Jamali et al., 2021), the author explored the potential of using a generative adversarial network (GAN) to address the challenge of insufficient labeled data for wetland classification. The results indicate that applying GAN techniques for generating and classifying wetland samples from Sentinel-1 and Sentinel-2 is effective. Furthermore, although some studies have compared ML and DL algorithms to demonstrate the advantages of DL-based methods over traditional ML techniques (Rezaee et al., 2018b; Mahdianpari et al., 2018), these comparisons are often conducted under inconsistent conditions.

Despite advancements in RS and ML, there is a notable absence of published research leveraging CNNs for peatland classification, particularly in the context of utilizing multi-sensor and multiresolution data. None of the above mentioned authors used such a complex input dataset as we are testing in this current paper. In addition, previous research in peatland classification has predominantly relied on traditional ML techniques, which often struggle to accurately delineate complex peatland features and exhibit limited scalability across diverse environments.

This study builds upon our previous conference papers (Farahnakian et al., 2023b,a) by expanding the results for peatland site type and fertility level classification at the pixel level. We investigate the application of CNN for pixel-level peatland classification, focusing on the development of a multi-modal CNN architecture. CNN was chosen for its ability to process high-dimensional data and capture complex spatial and contextual relationships, making them ideal for RS tasks like peatland classification. The summary of our main contributions is as follows:

(1) **Development of a Multi-Modal CNN Architecture:** We designed a CNN-based late fusion architecture that effectively integrates multi-source remote sensing (RS) data, including optical imagery, synthetic aperture radar (SAR), airborne laser scanning (ALS), and multi-source national forest inventory (MS-NFI) datasets. This integration maintains the spatial resolution of each data source, preserving crucial information for pixel-level peatland classification.
(2) **Optimization for High-Dimensional Data and Limited Samples:** To address the challenges of high-dimensional RS data and limited training samples, we adapted the Sequential Forward

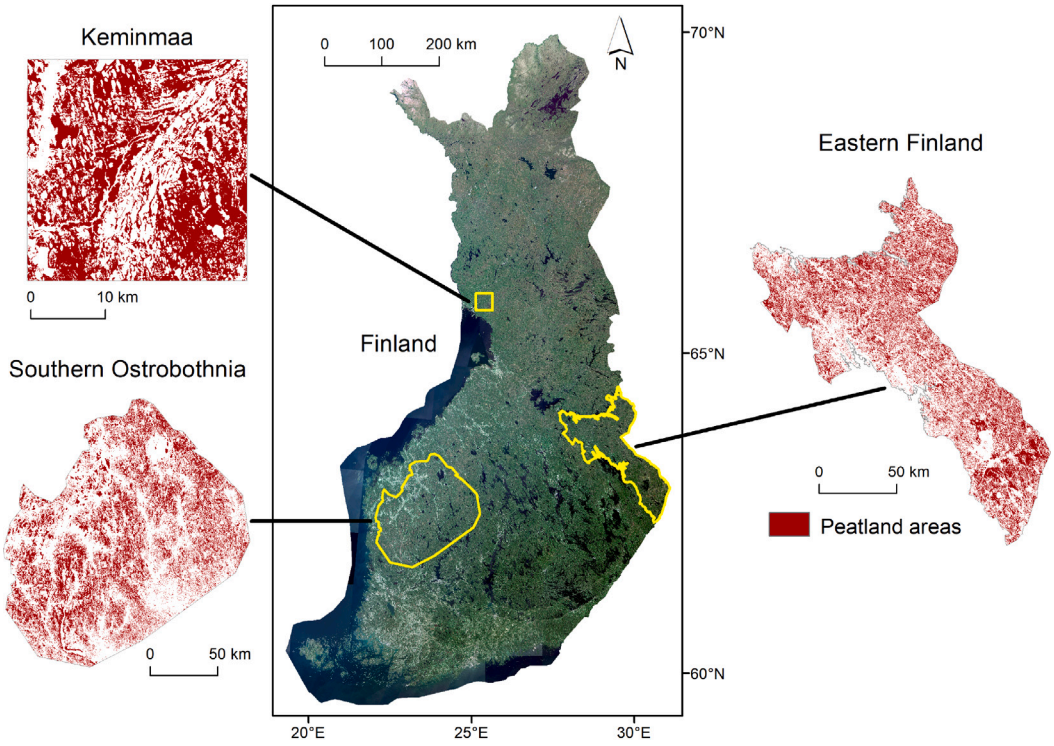

Fig. 1. Location of the study areas in Finland, including Keminmaa, Southern Ostrobothnia and Eastern Finland, displayed on a summertime Sentinel-2 mosaic true-color composite.

Selection (SFS) method to optimize feature selection. This adaptation reduces computational complexity and enhances model performance, mitigating overfitting.

(3) **Sliding-Window Method for Multi-Resolution Datasets:** We introduced a sliding-window methodology to manage multi-resolution datasets, ensuring that spatial and contextual relationships are preserved during pixel-wise classification.

(4) **Regularization Techniques for Overfitting Mitigation:** To further tackle overfitting, we incorporated L2 regularization and dropout mechanisms, enhancing the model's robustness and generalization capacity.

(5) **Nationwide Classification of Peatland Site Types and Land Use Categories:** The architecture was validated across three diverse study areas in Finland, enabling the nationwide classification of drained and undrained peatland site types, fertility classes, and land use categories, including active and abandoned arable lands on organic soils. The data used in this study were part of the Advances in Soil Information-MaaTi project (resources institute Finland (LUKE), 2021; Middleton et al., 2023).

(6) **Open-Source Contribution:** Our implementation, including code and models, is made publicly available on GitHub at https://github.com/MaaTi-project/Peatland-MultiSensor-CNN, supporting transparency and reproducibility for future research.

2. Study areas and data

In Finland, three study areas were selected including Keminmaa (Kemi), Southern Ostrobothnia (SO) and Eastern Finland (EF). As you can see in Fig. 1, the selected areas cover a variety of peatland vegetation zones and their site types in different fertility classes (Laine et al., 2018). Kemi is characterized by a wide variation in peatland site types related to southern aapa mires ranging from the most nutrient-rich minerotrophic to oligotrophic types. SO site is dominated by nutrient-poor site type of eccentric raised bogs and is heavily influenced by past peat extraction and has a high number of active and abandoned agricultural organic soil field plots. EF test area, compared on the two other sites has more topographic variation, a relatively lower number of training data represent- ing a typical area outside of the densely inventoried peatland regions, and posses a relatively higher portion (73%) of drained peatlands. For a more detailed description of the test areas see the technical report (Middleton et al., 2023).

Table 1 shows the characteristics of the input raster data. RADARSAT-2 and TerraSAR-X data were only available from the Kemi site. The spatial resolution column in the table represents the pixel size which the data was resampled to be used in this paper. The number of features is calculated by multiplying the number of rasters by the number of bands. For instance, there are five Sentinel-1 intensity images with two polarizations which totals 10 features for each study area. The data was used in this study can be divided into five main categories as follows:

2.1. Optical satellite data

Sentinel-2 (S2) satellite data were considered as the most appropriate optical data choice owing to its frequent acquisition, free availability, good spatial resolution and consistent spectral quality. Most of the applicable summertime images were downloaded from FinHub[1] service as Level-1C data and further converted to Level-2A using Sen2Cor processor, and part of the images from SciHub[2] service as readily processed Level-2A data. Features used for modeling included pixel values from all the bands with 10–20 m initial resolutions, where the 20 m bands were resampled to 10 m pixel size to enable production of single-file multi-band rasters. Only Kemi study area could fit completely inside a single S2 image tile, given its relatively small coverage. This facilitated the search of suitable images and one image per month between May and September, selectively from years 2018–2020, were applied as

[1] https://finhub.nsdc.fmi.fi/#/home.
[2] https://dataspace.copernicus.eu/.

input features. For Southern Ostrobothnia, the mosaic was based on 11 and for Eastern Finland 10 mainly cloudless and partially overlapping S2 tiles. These images were selected manually from all the available images acquired between June and August in 2019–2020. The two-year span was necessary for finding a full coverage of good quality images, and they were manually masked to exclude any remaining clouds and cloud shadows. Then, band-wise correction factors were calculated to each image by linear regression based on the overlapping pixel values, and the corrected images were merged into larger mosaics. This procedure was considered necessary for correcting deviations derived from atmospherical differences, regardless of utilizing Level-2A images which in principle should be atmospherically corrected.

2.2. Synthetic Aperture Radar (SAR) satellite data

Depending on the study area, three different SAR data sources were applied: Sentinel-1 images (all study areas), TerraSAR-X (only Kemi erraSAR-X, 2023) and RADARSAT-2 (only Kemi Ltd, 2018). TerraSAR-X (single look slant range complex mode, stripmap product) and RADARSAT-2 (SGF product) data consisted both of several seamless mosaics, acquired on different dates during the summer of 2017. They were calibrated and processed into dB values using the Sentinel Application Platform (SNAP), and terrain corrected with assistance of digital elevation model (2 m DEM of Finland (NLS), 2023).

With Sentinel-1 (S1) data we refer to backscattering intensity, derived from the ground range detected (GRD) products, and coherence images, calculated for image pairs based on the single look complex (SLC) products using SNAP software. Data from year 2017 were used for Kemi to match the other SAR data sources. At the other areas 2019 data was used. Both vertical transmit - vertical receive (VV) and vertical transmit - horizontal receive (VH) polarizations were applied as input features, as well as their division ratio. Five intensity images were used from each study area, one per month between May and September. For coherences, Kemi study area included 12 image pairs (May 23–Sep 26, 2017), Southern Ostrobothnia 11 pairs (May 22–Sep 25, 2019) and Eastern Finland 11 pairs (May 20–Sep 17, 2019), which were used to calculate coherence images both for consecutive passes of the same satellite (at 12-day intervals) as well as for longer temporal intervals by using always a single midsummer reference image as a "fixed" part of the pair. In addition, due to high degree of noise in the coherence data on Southern Ostrobothnia and Eastern Finland study areas, all the processed coherence image pairs on them were used to calculate pixel-wise maximum and average values of both VV and VH polarizations as well as for their ratio. For EF, only the average and maximum datasets were used. As you can see from Table 1, we have much fewer coherence layers for EF.

2.3. Airborne Laser Scanning (ALS) data and derivatives

The derived digital elevation models (DEM) by National Land Survey (NLS) (of Finland (NLS), 2023) and a canopy height model (CHM (Tuotekuvaus, 2022)) by the Finnish Forest Center were used as input features. These both were derived from ALS data, considering the last returns as the DEM, the first returns as a canopy model and their subtraction as the canopy height model (CHM). DEM data was available in 2 m pixel size and CHM data in 1 m pixel size, respectively. The DEM and CHM applied in the study were based on ALS data acquired between 2008 and 2019, following the newest available ALS data from each region. The relatively long time-span of the ALS acquisitions is known to be a potential source of local errors and causing mismatch with regards to the more recent S1 and S2 data. However, the data contains crucial information on the canopy structure, field layer vegetation structure and terrain microtopography such that it was considered a valuable data source and, therefore, was included in the analysis. In addition, local binary pattern (LBP) (Pietikäinen et al., 2011) derivatives from the DEM and CHM datasets, modeling textural patterns within pixel neighborhoods, were produced and used as input data.

2.4. Multi-Source National Forest Inventory (MS-NFI)

MS-NFI data[3] refers to periodically produced raster-based forest resource maps which cover forested land on both mineral and organic soils as well as treeless peatlands and clear-cuts (Mäkisara et al., 2022). Forest resource maps utilized in this study contained total volume of growing stock, volumes of pine, spruce, birch and other broad-leaved species, canopy cover, basal area, mean diameter, mean height, site type and main site type.

The principal contribution of forest resource maps for peatland classification is connected to the potential of a site for growing trees rather than its transient situation (e.g., straight after clearcut). Therefore, the MS-NFI maps of different years were overlaid and processed into their maximum (continuous variables), median (ordinal variables) or mode values (discrete variables). As it is unknown whether the most recent or past data describes the growing potential better, two different input feature layers were produced: one for years 2000–2011 (consisted of five distinct MS-NFI maps) and the other for 2013–2019 (four MS-NFI maps).

2.5. Field dataset

Separate training data sets were constructed for the drained and undrained subareas separately using a drainage mask raster created from the artificial drainage ditches stored in a topographic database by NLS (of Finland (NLS), 2023). This decision was made after rigorous testing to diminish miss-classification of site types between the drained and undrained areas. Training data was extracted from the Geological Survey of Finland (GTK) peatland inventory[4] and Luke NFI datasets,[5] which included point locations of the types of observed sites. In the GTK data, the site type was determined around the field observation location within a 25 m radius (Virtanen, 2020). Regarding to the NFI data, site type was defined using a minimum mapping unit of 0.25 ha which corresponded best to the nominal point location. Each observation site was visited in the field and their peatland site type was determined by qualified personnel. The observed site types followed the Finnish peatland classification system (Laine et al., 2018), which is based on the forest site type classification theory (Cajander, 1913). The classification utilizes site fertility and wetness as discrimination variables. Of the two main gradients used in the site classification, fertility is a more permanent property, but wetness can be affected by artificial drainage. Observations made after the year 2000 were selected from the databases such that the output map would contain information of the current site type. Table 2 shows the number of the training data of the site types at each of the study areas. The number of features n represents the total features (i.e. for Kemi (drained), $n = 146$) which are extracted from the whole data (optical, SAR, ALS and MS-NFI) and their bands.

Table 3 lists the peatland site type and fertility classes used in this work. Furthermore, it illustrates the corresponding fertility level of each peatland site type class. For instance, all original peatland site types corresponding to *Vaccinium myrtillus I* and *II* fertility levels are combined to one fertility class (fertility level 2). This was done to produce fertility level classes applicable directly to greenhouse gas inventory (Finland, 2022). This reduced the number of original site type classes into five main classes corresponding to the permanent fertility gradient of site type classification, which is not affected by the possible drainage of the site. Additionally three land use classes such as organic soil agricultural fields (OSAF) and abandoned fields on peat

[3] https://etsin.fairdata.fi/dataset/0c1ea04e-5ee3-410e-a954-1be27bda57d4.

[4] https://tupa.gtk.fi/paikkatieto/meta/tutkitut_turvealueet.html.

[5] https://etsin.fairdata.fi/dataset/58751432-d60f-40dd-a68f-2fa0708d47d2.

Table 1
Summary of datasets used in Peatland mapping, including optical and SAR satellite data, ALS-derived models, and forest inventory data. Each dataset is described by bands, original resolution, pixel size, and the number of features in each study area.

Data	Description	Original resolution (m)	Pixel size (m)	No. of features		
				Kemi	SO	EF
Sentinel-1 intensity	Microwave band C (5.5 cm) VV, VH	20 (VV, VH)	10	10	10	10
Sentinel-1 coherence	Microwave band C (5.5 cm) VV, VH	20 (VV, VH)	10	48	50	6
RADARSAT-2	Microwave band C (5.6 cm HH, HV)	10 (HH, HV)	10	10	–	–
TerraSAR-X	Microwave band X (3.1 cm/ HH)	2.5 (HH)	10	2	–	–
Sentinel-2 (S2)	B2 (490 nm), B3 (560 nm), B4 (665 nm), B5 (705 nm), B6 (740 nm), B7 (783 nm), B8 (842 nm), B8A (865 nm), B11 (1610 nm), B12 (2190 nm)	10–20 (multi-band)	10	50	10	10
Digital Elevation Models (DEM)	Terrain elevation above sea level	2	2	1	1	1
Canopy Height Model (CHM)	Canopy height model	1	1	1	1	1
Local Binary Pattern (LBP) for DEM	Derived from DEM	2	2	1	1	1
Local Binary Pattern (LBP) for CHM	Derived from CHM	1	1	1	1	1
Multi-Source National Forest Inventory (MS-NFI)	Forest resource maps	16	16	22	22	22

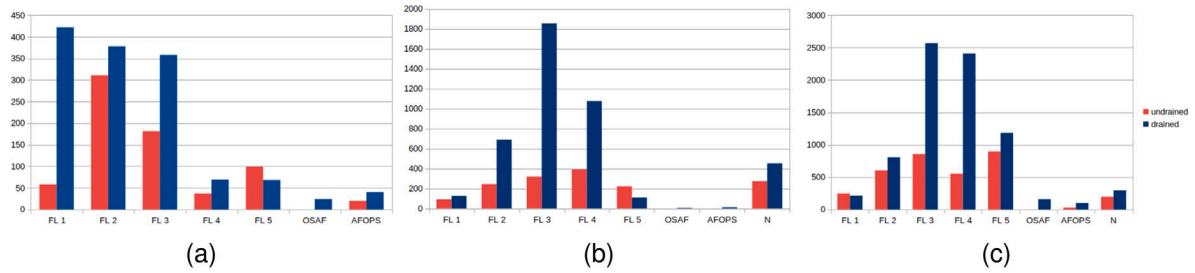

Fig. 2. Distribution of the fertility levels at (a) Kemi, (b) EF and (c) SO study areas for both drained and undrained subsections.

Table 2
Characteristics of the datasets in each study area.

Name of dataset	No. of peatland sit type classes	No. of fertility classes	Total no. of features
Kemi (drained)	36	7	146
Kemi (undrained)	36	7	146
SO (drained)	40	8	96
SO (undrained)	39	8	96
EF (drained)	39	8	52
EF (undrained)	35	8	52

soils (AFOPS), and mineral soil (negative, N) were used. Fig. 2 indicates the number of the training sites for the higher hierarchical level fertility classes in each study area, respectively.

Table 3 also shows the number of samples for each site type in three study areas. The last row of this table shows the total number of training points d (i.e., for Kemi drained, $d = 1367$). The distribution of the classes show two main challenges in our datasets. First, the site type dataset consists of a small set of training samples. Second, it has an imbalanced organization of class instances such as most real datasets usually do. For example, class "EHWSF" being rare only one sample in SO (undrained) and EF (drained) was available. The maximum number of sample belongs to the class "HRTHP I" and "TSF" which is 311 and 64 for Kemi drained and undrained classifications, respectively. In SO, the maximum number of samples for "VVITHP" and class "SFPB" are 1265 and 464 in drained and undrained classifications. For EF, the maximum number of samples belonging to the "VVITHP" is 902 and "LSB" only 144 for drained and undrained, respectively.

3. Methodology

The proposed methodology consists of two phases: feature selection and pixel-level classification. In the first phase, the most relevant features are identified to reduce overfitting and enhance model efficiency. In the second phase, pixel-level classification is performed using the selected features, assigning a specific peatland class label to each pixel and generating a classification map. Both phases utilize a multimodal CNN-based architecture, as illustrated in Fig. 3, designed to effectively integrate diverse data sources and preserve spatial and contextual information. In this section, we first present an overview of the proposed network. Next, the first phase (feature selection) is discussed based on the sequential forward selection algorithm. Then, the second phase of the methodology is described for pixel-level classification.

3.1. Architecture

The proposed architecture (Fig. 3) processes multi-resolution data separately through three streams, each designed to independently extract features from different input sources with varying spatial resolutions. The outputs from each stream are then concatenated to generate a final classification map, leveraging a late or decision-level fusion approach. This architecture preserves all possible information from the multi-resolution features, avoiding interpolation that might otherwise result in the loss of critical details. The design captures the unique resolution and semantic scales of the features, striking a balance between model complexity, training sample size, and class variability.

Each stream in the architecture consists of two convolutional layers, two pooling layers, and one fully connected layer. The size of the CNN

Table 3
Fertility levels and peatland site type classes according to Laine et al. (2018) and Päivänen and Hånell (2012), and number of observations and their abbreviations for Kemi, SO and EF.

Fertility class	Description of fertility class	Original peatland site type	No. samples						Abbreviation
			Kemi		SO		EF		
			Drained	Undrained	Drained	Undrained	Drained	Undrained	
1	Herb rich type/Oxalis-Myrtillus type	Eutropthic paludified hardwood-spruce forest	9	3	1	4	2	1	EPHSF
1	Herb rich type/Oxalis-Myrtillus type	Herb-rich hardwood-spruce swamp	80	22	20	16	29	34	HRHSS
1	Herb rich type/Oxalis-Myrtillus type	Herb-rich sedge hardwood-spruce fen	2	2	2	1	5	4	HRSHSF
1	Herb rich type/Oxalis-Myrtillus type	Herb-rich type heathy peatland I	311	24	187	224	87	52	HRTHP I
1	Herb rich type/Oxalis-Myrtillus type	Herb-rich type heathy peatland II	0	0	1	0	0	0	HRTHP II
1	Herb rich type/Oxalis-Myrtillus type	Eutrophic hard-wood-spruce fen	0	0	0	1	1	0	EHWSF
1	Herb rich type/Oxalis-Myrtillus type	Eutrophic birch fen	19	7	0	0	2	1	EBF
2	Vaccinium myrtillus type I	Paludified Vacc. myrtillus spruce forest	71	57	41	46	29	42	PVMSF
2	Vaccinium myrtillus type I	Vacc. myrtillus spruce swamp	40	42	27	54	50	67	VMSS
2	Vaccinium myrtillus type I	Vacc. myrtillus type heathy peatland I	65	7	419	275	304	82	VMTHP I
2	Vaccinium myrtillus type I	Herb-rich sedge fen	19	28	12	29	16	14	HRSF
2	Vaccinium myrtillus type II	Eutrophic fen	9	18	1	1	1	0	EF
2	Vaccinium myrtillus type II	Eutrophic flark fen	16	45	0	0	0	1	EFF
2	Vaccinium myrtillus type II	Herb-rich flark fen	18	42	2	4	17	5	HRFF
2	Vaccinium myrtillus type II	Herb-rich sedge brich-pin fen	58	20	69	20	146	13	HRSBPF
2	Vaccinium myrtillus type II	Eutrophic pine fen	22	22	0	4	3	4	EPF
2	Vaccinium myrtillus type II	Tall-sedge hardwood-spruce fen	44	29	4	4	10	3	TSHSF
2	Vaccinium myrtillus type II	Vacc. myrtillus type heathy peatland II	16	1	231	166	112	13	VMTHP
3	Vaccinium vitis-idaea type I	Vacc. vitis-idaea spruce swamp	31	3	14	24	10	10	VVISS
3	Vaccinium vitis-idaea type I	Spruce-pine swamp	3	4	49	37	161	27	SPS
3	Vaccinium vitis-idaea type I	Paludified pine forest	14	32	123	105	41	46	PPF
3	Vaccinium vitis-idaea type I	C. globularis pine fen	44	18	96	29	63	35	CGPF
3	Vaccinium vitis-idaea type I	C. globularis spruce swamp	40	6	1	4	0	0	CGSS
3	Vaccinium vitis-idaea type I	Vacc. vitis-idaea type heathy peatland I	0	0	1265	360	902	62	VVITHP I
3	Vaccinium vitis-idaea type II	Flark fen	6	16	10	7	16	4	FF
3	Vaccinium vitis-idaea type II	Cottongrass-sedge pine fen	0	1	3	8	3	21	CSPF
3	Vaccinium vitis-idaea type II	Tall-sedge fen	25	64	20	56	40	54	TSF
3	Vaccinium vitis-idaea type II	Tall-sedge pine fen	21	13	433	52	458	54	TSPF
3	Vaccinium vitis-idaea type II	Vacc. vitis-idaea type heathy peatland II	106	15	555	174	159	7	VVITHP II
4	Dwarf shrub type	Dwarf scrub pine bog	17	4	912	192	96	72	DSPB
4	Dwarf shrub type	Dwarf shrub type heathy peatland I	31	1	864	91	476	28	DSTHP I
4	Dwarf shrub type	Dwarf shrub type heathy peatland II	0	0	9	0	0	0	DSTHP II
4	Dwarf shrub type	Low-sedge S. papillosum fen	14	17	7	31	22	103	LSSPF
4	Dwarf shrub type	Cottongrass pine fen	14	15	544	143	322	129	CPF
4	Dwarf shrub type	Low-sedge pine fen	2	0	74	95	160	59	LSPF
5	Cladina type	S. fuscum pine bog	20	18	1014	464	60	41	SFPB
5	Cladina type	Cladina type heathy peatland I	0	0	70	4	10	0	CTHP I
5	Cladina type	Cladina type heathy peatland I	0	0	1	0	0	0	CTHP II
5	Cladina type	S. fuscum bog	46	55	24	138	2	13	SFB
5	Cladina type	Ridge-hollow pine bog	0	1	42	150	2	24	RHPB
5	Cladina type	Low-sedge bog	2	25	33	140	36	144	LSB
Abandoned field on peat soils	Abandoned field on peat soils	Abandoned field on peat soils	40	20	97	31	13	0	AFOPS
Organic soil agricultural fields	Organic soil agricultural fields	Organic soil agricultural fields	24	0	157	1	7	0	OSAF
Non-peatland	Non-peatland	Negative (mineral soils)	0	0	293	198	453	274	N
–	–	–	1376	706	7727	3383	4326	1543	–

input in each stream is determined by the total number of bands × row (width) × column (height), where the number of bands corresponds to the input variables for each stream. Convolutional layers utilize kernels tailored to the spatial resolution of the input data. For example, in *Stream1* and *Stream3*, a kernel size of 5 × 5 is applied, while *Stream2* employs a larger kernel size of 25 × 25 to accommodate coarser resolution data.

Each convolutional layer is followed by a Rectified Linear Unit (ReLU) activation function, batch normalization (Ioffe and Szegedy, 2015), and a dropout layer (Krizhevsky et al., 2012b). Batch normalization enhances training stability, while dropout layers with a 10% probability reduce overfitting. Max-pooling is performed on each feature map using a 2 × 2 kernel with a stride of 1, maintaining high spatial resolution. After convolution and pooling, the resulting feature maps are flattened into 1-D vectors for each stream, which are then concatenated along the channel axis. Finally, a softmax activation function extracts class probabilities for multi-class classification. The late fusion strategy combines rich semantic information from all input sources.

Additionally, a window-based approach is employed to train the CNN architecture. This method defines an $n \times n$ window around each training data point, centering the point within the window. Commonly used in image classification (Hodgson, 1998), this approach reduces computational time and mitigates overfitting by restricting analysis to a limited number of features within the window. The window size varies according to the spatial resolution of the input data to cover an approximate area of 50 m in squares, corresponding to the field-observed ground truth area. For instance, a window size of $n = 5$ is used for inputs with 10 m and 16 m pixel resolutions (see Table 1). For the high-resolution data (1 m resolution), the window size is 25 × 25 meters, which is equivalent to 25 × 25 pixels.

3.2. Feature selection

To avoid overfitting, we propose a modified version of the sequential forward selection (SFS) (Marcano-Cedeño et al., 2010) to select relevant features for the pixel-level classification phase. SFS is widely used due to its simplicity and speed. The original SFS algorithm follows a bottom-up search approach. Features are added sequentially into an empty set, I, based on an objective function that maximizes classification accuracy. At each step, a single feature from the remaining pool is added to the set I, and the performance is evaluated. In the next iteration, SFS adds the new input i and evaluates the classifier with this combination and the remaining features. This process is repeated until all possible combinations have been tested, and the best input set is selected.

To reduce computational and time complexity, we modify SFS to consider only the best input from each data type with the same spatial resolution, rather than evaluating all features in every round. For example, in the first step, the input with the highest performance may be the channel B5 from the S2 ($S2_{B5}$). In the second step, we combine $S2_{B5}$ with the best features from each spatial resolution (*Stream1* to 3) to select the top two features. These two features may come from the same stream (e.g., *Stream1*) or from different streams (e.g., one from Stream 1 and one from *Stream2*, or one from Stream 1 and one from *Stream3*). This process is repeated until all combinations of the best data types are trained and tested. In the final step, the proposed CNN is trained on the full dataset based on the selected features.

3.3. Pixel-level classification

To generate the classification map each center pixel of the predefined $n \times n$ pixel size window is labeled with the proposed CNN. Then the features in the entire window are extracted separately from each stream and after that the class predictions from each individual stream

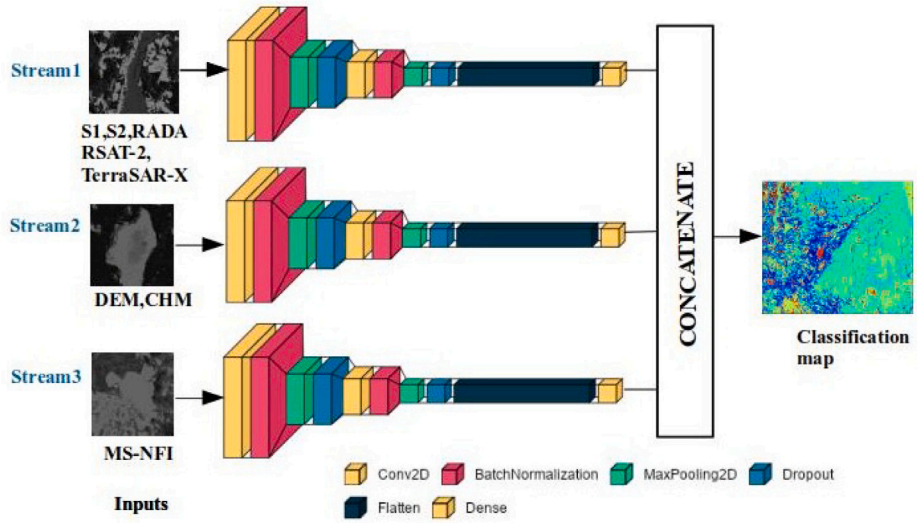

Fig. 3. The proposed multimodal CNN fusion architecture for pixel-level classification of peatland site types.

are combined by concatenating them. The final output is a classification map with a spatial resolution of 10 m, where each pixel is assigned to a specific peatland site type class. In addition, each site type class is reclassified into the corresponding fertility level (higher hierarchical class, see Table 3) in order to generate the classification map for this level with the same resolution.

3.4. Implementation details

All the experiments were implemented using Tensorflow2.9.1, Keras2.9.0 and Python3.9. We also used 5-fold Stratified Cross Validation (SCV) (Zeng and Martinez, 2001) technique to ensures that each fold of a dataset has the same distribution of classes to address the class imbalance problem. This is particularly useful when dealing with imbalanced datasets, where some classes have significantly fewer samples. The dataset was split into three subsets: Training, Validation (for SCV), and an independent Test Set. The independent test set was completely excluded from both training and validation phases.

To update network weights, we use Adam (Farahnakian et al., 2018) as an optimization algorithm and the learning rate of 0.001. The model was trained for a total of 500 epochs. During each epoch, the model was trained on a batch of 128 samples and its parameters were updated based on the optimization algorithm and a used loss function. We also use cross-entropy loss with a softmax layer in the end. In order to reduce overfitting, L2 regularization with the rate of change 0.06 is assumed. In addition, dropout as another main regularization methods is used after each pooling layer to improve generalization and performance of CNN on unseen data.

To address the potential problem of overfitting caused by limited training samples, we also applied data augmentation to generate 50% more training samples by random rotation, vertical and horizontal flips. This data augmentation methodology is particularly useful for RS data (Li et al., 2018).

3.5. Evaluation metrics

To evaluate the performance of our proposed model, we calculate the overall accuracy, precision, recall, F1-score and Kappa value for site types classes and fertility levels. Final performance metrics were computed based on the independent test set to validate the generalization capability of the model. The F1-score is a measure of the balance between precision and recall, influenced by both false positives and false negatives, and it is calculated as follows:

$$F1 = 2 \times \frac{precision \times recall}{precision + recall} \tag{1}$$

In addition, precision and recall are defined as:

$$Precision = \frac{1}{N}\sum_{k=1}^{N}\frac{TP_k}{TP_k + FP_k} \tag{2}$$

$$Recall = \frac{1}{N}\sum_{k=1}^{N}\frac{TP_k}{TP_k + FN_k} \tag{3}$$

where TP_k, FP_k, TN_k and FN_k indicate the number of true positive, false positive, true negative, and false negative pixels for an object indexed as class k, respectively.

4. Results

4.1. Feature selection

Table 4 summaries the feature selection results that we got from our SFS approach. It shows the accuracy gained with the best input from each data source at each study area. From these results, we can answer two main research questions: (1) which data source and (2) feature of each data source provide the most relevant information to the peatland site type classification at each study area. From the results in Table 4, the highest accuracy (33.8%) is achieved for the SO undrained data with the S2 data source. Comparison of different data acquisition times was only conducted at Kemi, and the results show that S2 imagery acquired July provided the highest accuracy compared the other data acquisition times in May, June, August and September. S2 data is the most appropriate data source of all input sources for classifying peatland site types because it provides the highest classification accuracies at all study areas (Table 4). The relevance of S2 derives from multiple wavelengths (bands), including also the short-wave infrared, which contains most important information for distinguishing peatland site types.

The results (Table 4) show that both S1 intensity and coherence are important for peatland site type classification. No unanimity can be seen when comparing the acquisition times of intensity data. What comes to S1 coherence features, the most commonly selected single-image coherence pairs are those consecutive ones (with 12-day interval) rather than the ones with longer interval. The shorter time lag between image pairs produces high quality signal with less noise which in the case of the peatland site types produced better separability of the classes than the long-time interval coherence. In addition to S1, also CHM and MS-NFI were relevant contributors to the classification. However, the DEM produced over 20% accuracies only with the Kemi drained but not for the other study areas. This indicates that of all input

Table 4
Accuracy of the best input for each data type in each study area (drained and undrained).

Data	Kemi				SO				EF			
	Undrained	Acc	Drained	Acc	UnDrained	Acc	Drained	Acc	Undrained	Acc	Drained	Acc
S1 intensity	VV/VH, Aug 3th, 2017	23.8	VV/VH, May 23th, 2017	20.1	VV/VH, Aug 26th, 2019	18.9	VV/VH, Aug 26th, 2019	22.6	VV/VH, May20th, 2019	15.1	VV/VH, July 19th, 2019	25.5
S1 coherence	VV/VH, Maximum coherence from multiple 2019 images	23.1	VV/VH, Maximum coherence from multiple 2019 images	18.5	VV/VH, May 11th–May 23th, 2019	23.1	VV/VH, Maximum coherence from multiple 2019 images	22.3	VV/VH, Maximum coherence from multiple 2019 images	22.4	VV/VH, Maximum coherence from multiple 2019 images	27.8
RADARSAT-2	HH/HV, Aug 4th, 2017	18.0	HH/HV, Aug 4th, 2017	18.2	–	–	–	–	–	–	–	–
TerraSAR-X	HH, May 30th–Jun 5th, 2017	21.9	HH, May 30th–Jun 5th, 2017	18.9	–	–	–	–	–	–	–	–
S2	Jul 18th, 2018	**25.7**	Jul 18th, 2018	**26.8**	Mosaic from good-quality summer 2020 images	**33.8**	Mosaic from good-quality summer 2020 images	**33.3**	Mosaic from good-quality summer 2019–2020 images	**26.3**	Mosaic from good-quality summer 2019–2020 images	**30.9**
DEM	DEM	11.1	DEM	21.7	DEM	16.7	DEM	7.7	DEM	18.0	DEM	17.4
CHM	CHM	25.2	CHM	22.5	CHM	22.8	CHM	14.6	CHM	23.1	CHM	30.5
MS-NFI	Mean diameter for years 2000–2011	22.1	Site type median for years 2013–2019	25.9	Site type median for years 2013–2019	26.9	Site type median for years 2013-2019	21.8	Mean tree diameter for years 2000-2011	22.6	Mean tree diameter for years 2000–2011	27.4

Table 5
The selected features for three study areas. The features are ranked from the top to bottom based on their importance for each study area. The column 'Accuracy' shows how the CNN performs in terms of accuracy when trained using the current feature along with the previously selected features.

Name of dataset	Feature description (data type, raster layer and date)	Accuracy (%)
Kemi (undrained)	Sentinel-2 optical satellite data, July 18th, 2018	25.78
	LBP derived from CHM	26.20
	DEM	27.34
	TerraSAR-X SAR satellite data, HH, May 30th–Jun 5th, 2017	31.58
	MS-NFI, mean diameter for years 2000–2011	30.74
	CHM	31.44
Kemi (drained)	Sentinel-2 optical satellite data, Jun 19th, 2020	26.71
	Sentinel-1 SAR satellite data, VV/VH, coherence Sep 18th/Sep 30th, 2017	28.91
	RADARSAT-2 SAR satellite data, HV/HH, Sep 21th, 2017	31.64
	TerraSAR-X SAR satellite data, HH, May 30th–Jun 5th, 2017	33.03
	Sentinel-1 SAR satellite data, VV/VH, coherence Jul 20th/Sep 18th, 2017	33.62
	Sentinel-1 SAR satellite data, VV/VH, intensity Aug 3rd, 2017	32.67
	LBP derived from DEM	32.00
	DEM	32.74
	CHM	32.45
	MS-NFI, site type median for years 2000–2011	32.74
SO (undrained)	Sentinel-2 optical satellite data, mosaic from good-quality summer 2020 images	33.38
	Sentinel-1 SAR satellite data, VV/VH, averaged coherence from multiple 2019 images	32.18
	Sentinel-1 SAR satellite data, VV/VH, intensity May 22nd, 2019	33.25
	Sentinel-1 SAR satellite data, VV/VH, coherence Jul 10th/Jul 22nd, 2019	33.75
	Sentinel-1 SAR satellite data, VV/VH, intensity Sep 25th, 2019	33.81
	Sentinel-1 SAR satellite data, VV/VH, coherence Jun 28th/Jul 10th, 2019	32.86
	CHM	33.19
	MS-NFI, site type median for years 2013–2019	33.28
SO (drained)	Sentinel-2 optical satellite data, mosaic from good-quality summer 2020 images	32.18
	Sentinel-1 SAR satellite data, VV/VH, coherence Jul 10th/Jul 22nd, 2019	32.81
	Sentinel-1 SAR satellite data, VV/VH, averaged coherence from multiple 2019 images	33.33
	Sentinel-1 SAR satellite data, VV/VH, maximum coherence from multiple 2019 images	30.77
	Sentinel-1 SAR satellite data, VV/VH, intensity Sep 25th, 2019	32.57
	MS-NFI, site type median for years 2013–2019	31.21
	CHM	33.32
EF (undrained)	Sentinel-2 optical satellite data, mosaic from good-quality summer 2019–2020 images	26.32
	Sentinel-1 SAR satellite data, VV/VH, intensity Jul 19th, 2019	27.15
	Sentinel-1 SAR satellite data, VV/VH, maximum coherence from multiple 2019 images	28.06
	MS-NFI, mean tree diameter for years 2000–2011	28.77
EF (drained)	Sentinel-2 optical satellite data, mosaic from good-quality summer 2019–2020 images	30.98
	Sentinel-1 SAR satellite data, VV/VH, intensity Jul 19th, 2019	30.97
	Sentinel-1 SAR satellite data, VV/VH, maximum coherence from multiple 2019 images	31.56
	Sentinel-1 SAR satellite data, VV/VH, averaged coherence from multiple 2019 images	30.91
	MS-NFI, mean tree diameter for years 2000–2011	31.88
	DEM	31.11

Table 6
The classification performance metrics (%) of each study area for site types classification.

Study area	Kemi		SO		EF	
	Undrained	Drained	Undrained	Drained	Undrained	Drained
Accuracy	31.8	33.6	32.8	32.5	31.8	29.6
Precision	11.9	13.9	12.9	13.9	9.6	7.8
Recall	13.9	12.9	14.7	13.7	10.6	7.9
F1-score	12.3	13.9	14.2	13.2	10.0	7.8

Table 7
The classification performance metrics (%) of each study area for fertility level classification.

Study area	Kemi		SO		EF	
	Undrained	Drained	Undrained	Drained	Undrained	Drained
Accuracy	55.0	48.1	52.8	50.7	47.2	36.6
Precision	44.2	40.3	43.3	39.0	32.7	28.7
Recall	42.3	35.3	45.7	39.2	35.3	21.1
F1	43.2	41.2	44.4	39.0	33.9	24.3

data sources the 2 m DEM contains the least amount of information for site type separation. The elevational variation captured in the 2 m DEM (created of > 0.5 points/m^2 ALS point cloud) maybe too coarse for the class separation. Similarly to DEM, TerraSAR-X and RADARSAT-2 data had minor relevance to the classification success. Then the feature selection task was continued with only these best features which are mentioned in Table 4 in order to reduce the running time and computational complexities. In this table, the features are ranked from top to bottom based on the performance improvement.

In addition, Table 5 illustrates the selected features for each study area. It indicates which features distinguish the peatland site types most efficiently, i.e. the selected features produce the highest classification accuracy. Another observation from this table is the features are ranked based on their importance or relevance from top to down rows in each area. For example in Kemi (undrained), first the input S2 is selected and in the second round the combination of S2+ LBP of CHM produce the highest accuracy between all combination of two features. The result shows that the features such as S2 and S1 are selected in all sites. SAR data (S1) are sensitive to both soil moisture as well as surface roughness, and therefore provides complementary information to optical data in peatland site type classification. In most study areas, CHM is also selected. Characterization of the forested site types is based on tree species recognition and canopy tree height (Laine et al., 2018), and this information is retained in the CHM data. At EF, mean tree diameter from the MS-NFI layers was selected instead of CHM, proving the relevance of MS-NFI data as an input variable. The 2 m DEM (and LBP of DEM) was selected for Kemi and EF drained areas as one of the important features but not for other areas. In Kemi and OS, CHM was selected, and at Kemi drained also the LBP of CHM. Even though the LBP is derived from the CHM, it still contributes to improving the accuracy of site type recognition. This suggests that providing textural information to the CNN can be beneficial. Simply using the raw DEM or CHM may not be sufficient for the site type classification task in this application, especially given the limited training data and the high number of classes.

In addition, Fig. 4 shows the evolution of the classification accuracy for each area based on the selected features. For example, S2 data acquired in July 18th, 2018, is the best input between all S2 features as it is provide e.g. 25.7% accuracy for the Kemi undrained. But the accuracy is increased by 2.2% when CHM is added into the input space. The x-axis shows the number of input sources which are included to perform classification. Besides EF, up to 10 features are required to produce the maximum overall accuracy. For the EF, we have 8 input sources (see Table 1). From Fig. 4 it can be seen that the maximum accuracy (33.6%) is obtained with 10 input sources for Kemi (drained) that are listed in the first row of Table 5 from top to bottom (S2+LBP+DEM+ TerraSAR-X+ MS-NFI+CHM).

Overall, all input data sources retain information on separating the peatland site type classes. However, CHM, Sentinel-2 bands, and Sentinel-1 bands exhibit the highest importance, signifying their relevance in distinguishing between peatland site types.

4.2. Performance metrics

Table 6 and (Table 7) summarize the performance metrics for each study area based on the selected features for peatland site type and fertility level classification, respectively. Four observations can be drawn from the results:

(1) The accuracy for site type classifications are poor varying 31.8–33.6% for the undrained and 29.6–31.8% for the drained classifications (Table 6). The main reason is the limited labeled training samples and high number of site type classes.
(2) The fertility level classification accuracy varying 47.2–55.0% for the undrained and 36.6–50.1% for the drained (Table 7). For example, the accuracy is increased from 33.6% into 55.0% when we change the level of classification from peatland site type to fertility level for Kemi (undrained). The higher number of observations and lower number of classes in the fertility level classification most likely contributes to its better performance over the site type level classification.
(3) The highest total accuracy was gained with the Kemi (undrained) data for both classification levels. At Kemi, a relatively lower portion of the peatlands are drained for forestry (51.5%) compared to the other study sites (EF 74.2%, SO 83.0%). Thus, the Kemi training set contains relative more undrained peatlands which are more readily identifiable from RS data than the tree canopy covered peatlands. In addition, at Kemi, the fertile site types (fertility level 1, Fig. 2) are relatively more abundant compared to other two study sites. They are more distinguishable from the less fertile types in RS data because of their abundance of vascular plant and grass species covering the other mostly moss and sedge dominated fertility classes.
(4) F1-scores indicate that SO performs better in terms of balancing precision and recall. The classifier for this study area achieves both the highest precision (low false positive rate) and recall (low false negative rate) which may be caused by the higher number of training data compared to the other areas (see Table 2). However, the relatively low precision, recall, and F1-scores in other areas suggest that there may be an insufficient amount of training data for these areas, which could limit the model's ability to generalize effectively.

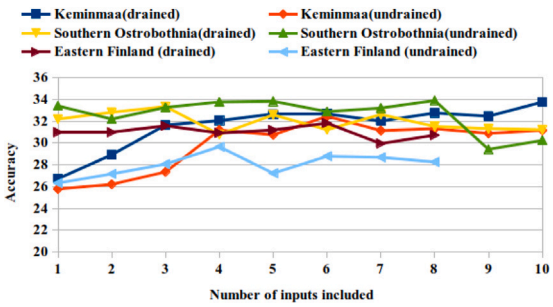

Fig. 4. Evolution of classification accuracy using the modified version of Sequential Forward Selection (SFS) across all study areas. The selected features are ranked in Table 5 before the accuracy begins to decrease.

4.3. Confusion matrix

The confusion matrices are generated in two levels: site types and fertility levels. Fig. 5 shows the confusion matrix for peatland site type classes. The results in Fig. 5(a) and (b) show that the maximum correct observations belongs to classes that we have more training samples such "HRTHP I" and "TSF" in Kemi drained and undrained datasets, respectively. For SO, we obtained the highest correctly labeled results for classes "SFPB", "VVITHP I" in undrained and drained as shown in Fig. 5(c) and (d). In EF (Fig. 5(e) and (f)), the highest correct observations belong to the classes "N", "VVITHP I" in undrained and drained.

Fig. 6 illustrates the confusion matrices for peatland fertility levels for all study area. These results show that maximum correct predictions belongs to FL1 and FL2 for Kemi drained and undrained, respectively. For SO (Fig. 6(c) and (d)), the class OSAF and FL5 has the maximum number of correct prediction. These classes are dominating in terms of number of observations (see Fig. 2). It is noteworthy that at OS and EF (undrained) many classes are falsely classified as the mineral soil class (N). The class is very versatile being composed of variety of peatyland type of vegetation, thus making it difficult to distinguish from other site types with RS .

4.4. Qualitative results

To further illustrate the ability of our model to effectively acquire peatland semantic information for site types and fertility levels, we visualized the classification maps for each study area. Figs. 7 and 8 show the prediction maps for site types and fertility levels in both drained and undrained, respectively. In addition, they illustrate the classification maps for three selected subsections of each study area. Although the classification accuracies are low to moderate the spatial patterns, however, are continuous and coherent.

5. Discussion

The integration of RS and ML techniques, particularly deep learning, provides significant solutions for land cover mapping. However, generating accurate maps of complex vegetation structures, such as peatlands, remains challenging. In this study, the application of CNN for peatland site type (37 classes) and fertility classification (5 classes), following the Finnish peatland classification scheme in Laine et al. (2018) by using variety of RS data and forest resource GIS data was investigated. To avoid information loss caused by the variable input raster data resolutions, we proposed a simple CNN-based fusion architecture that is able to process each data separately with the original spatial resolution. The proposed CNN architecture can combine multi-source geospatial data. We evaluated our architecture using data from three study areas in Finland. These regions represent different peatland site types and fertility levels, demonstrating the model's generalization capability. However, our approach provides a methodological framework that can be applied to broader regions, including other parts of Finland and similar landscapes globally. The main lessons from the experiments are as follows:

- The accuracy of CNN for peatland classification can be improved by adding the relevant features from all tested data sources including satellite optical, SAR, ALS and forest resource maps. As an example, the accuracy for peatland site type classification is improved 6.9% at Kemi (drained) when we added four other relevant features. The observation supports the findings of many studies highlighting the importance of many remotely sensed data sources to map the complex boreal peatland vegetation patterns successfully (Chasmer et al., 2020; Bourgeau-Chavez et al., 2016; Räsänen et al., 2020).
- Input feature selection shows that Sentinel-2 data is the most important data source in separating the site types at all study areas. Such conclusion, to the knowledge of the authors, has not been previously drawn regarding boreal peatland site type classification. Optical data separates the habitat classes according to the spectral characteristics of the dominant moss, sedge, dwarf shrub and tree species (Ustin et al., 2009; Peltoniemi et al., 2005; Harris et al., 2006; Middleton et al., 2012). If allowed by the availability of Sentinel-2 images, incorporating data on phenological variation during the growing season could further improve the results (Pang et al., 2023).
- Our experimental results across three different study areas, which encompass a variety of peatland vegetation, demonstrate the generalization ability of CNN for this task. Previous applications of deep learning in boreal peatland classification have been limited, such as in Chasmer et al. (2020), where six wetland community classes were classified with an accuracy of 93.12% in the Northwest Territories, Canada, using multi-spectral nano-satellite data. This study highlights the success of applying CNNs to fewer classes where more training samples are available for each class.
- The low number and imbalance of the training data poses a challenge for any ML approach including the CNN. The current study solely focused on recognition of the Finnish site types classification system according to Laine et al. (2018) and relevant fertility levels to serve the national green house inventory (Liao et al., 2020). In future work the focus should be on class content optimization (see e.g. Middleton et al. (2012)) to demonstrate the full capacity of RS in peatland mapping.
- When site types were reclassified to the higher level thematic fertility classes the classification accuracy was significantly improved. For example in Kemi (undrained) the accuracy is increased from 33.6% to 55.0%. In the fertility level classification into 5 classes the dominant species can be distinguished more readily with RS and forest resource data than the site types which have relatively smaller differences in vegetation abundance and structure than the fertility classes. Our result coincides with the previous studies stating that RS classification of boreal peatlands into vegetation community classes has been highly successful in many studies (Chasmer et al., 2020).
- For some site type classes such as VVITHP, we got better accuracy as the number of training samples are more than the number of other classes in SO and EF.
- To showcase the ability of the CNN in peatland site type classification would require increasing the number of observations in a training set (Li et al., 2019). The aim of the current work was in classification of peatland site types at national level. Thus, very high resolution, hyperspectral or polarimetric L-band SAR data such as demonstrated in Middleton et al. (2012), Räsänen et al. (2020) and Touzi et al. (2019) were not considered as input data sources. Our results, however confirm that additional data sources are required to facilitate the classification performance.

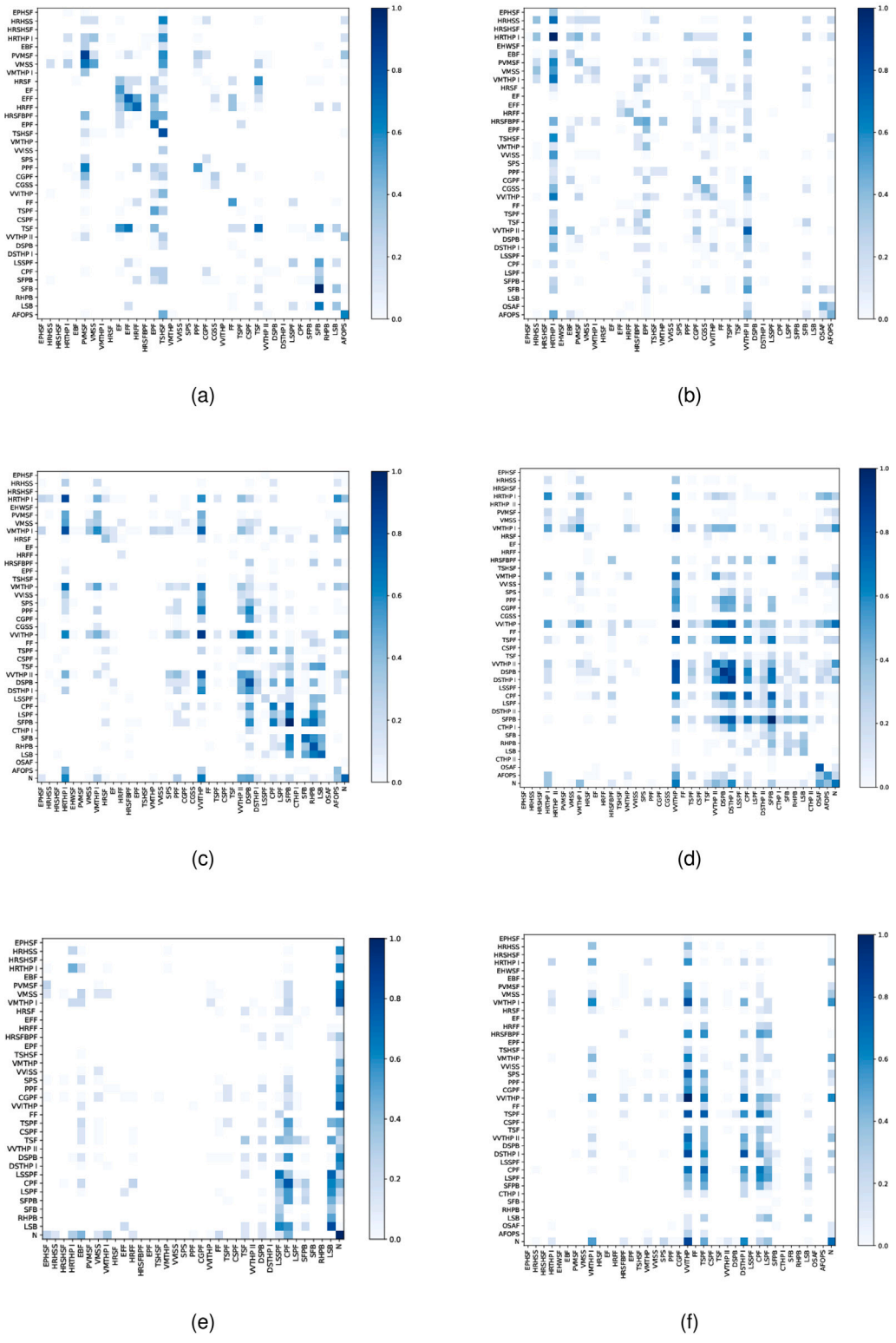

Fig. 5. The confusion matrix of site types classification for (a) Kemi undrained, (b) Kemi drained, (c) SO undraiend, (d) SO drained, (e) EF undrained and (f) EF drained. The rows in confusion matrix represent the actual class labels, and the columns represent the predicted class labels.

Generally, our findings from this study demonstrate that accurate peatland pixel-level classification require the most relevant features and that feature selection has a value for the peatland site type mapping. Comparing deep learning approaches to traditional statistical inference methods, we observe distinct trade-offs. While traditional methods often rely on predefined assumptions and simpler relationships, CNNs automatically learn hierarchical features from the data, reducing the reliance on manual feature engineering. However, several factors could potentially improve the results, and there were some limitations as outlined below:

- Limited Training Data: The model's performance is constrained by the limited availability of labeled training samples for certain

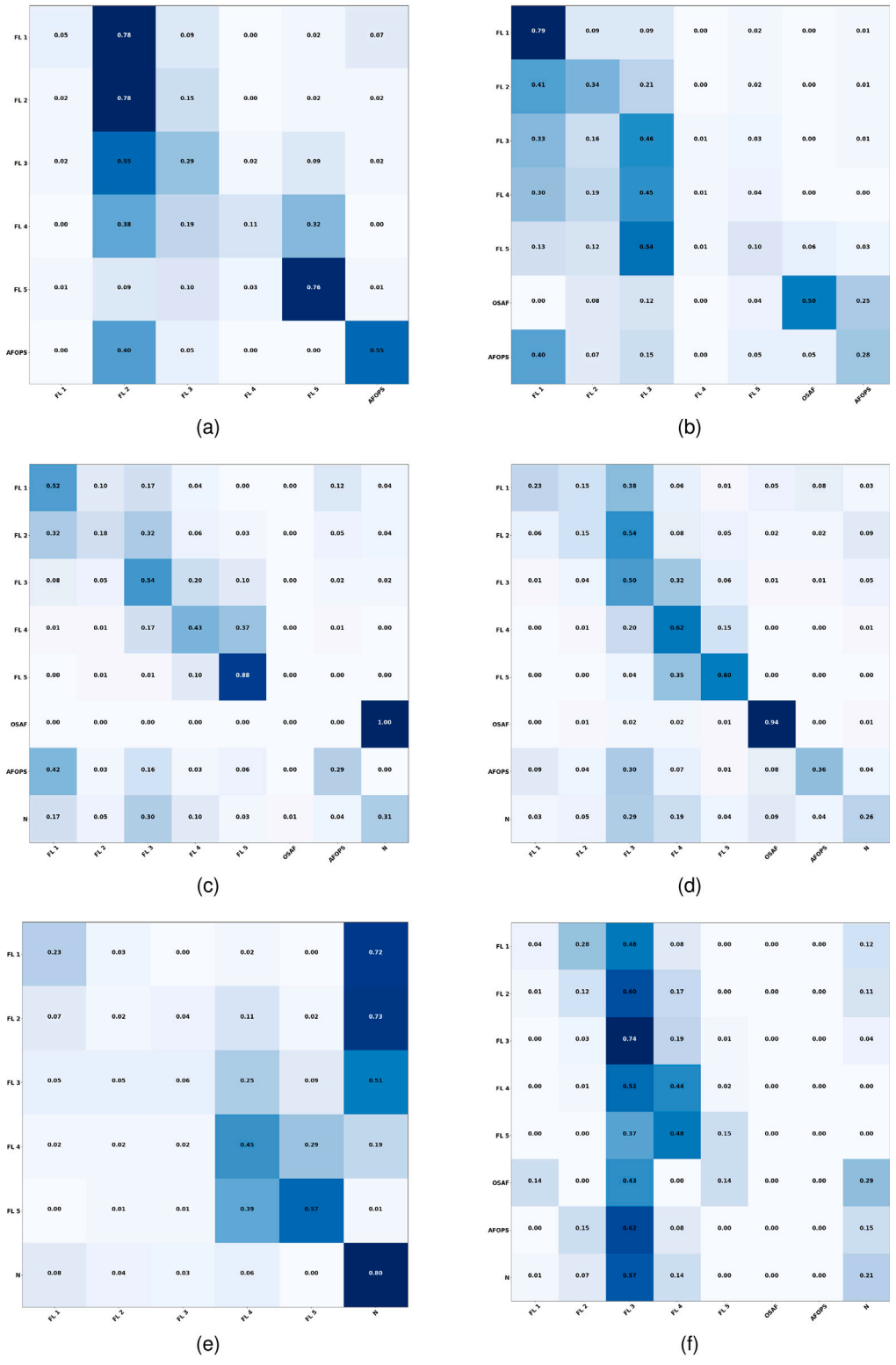

Fig. 6. The confusion matrix of fertility level classification for (a) Kemi undrained, (b) Kemi driand, (c) SO undraiend, (d) SO drained, (e) EF undrained and (f) EF drained. Figure arrangement the same as in Fig. 6.

peatland site types, particularly in the undrained categories. The imbalance in class distribution also affected classification accuracy. Future work will focus on data augmentation techniques and the incorporation of synthetic samples generated by Generative Adversarial Networks (GANs) to improve class representation.

- Spatial and Temporal Variability: Peatland ecosystems are dynamic and exhibit temporal changes due to seasonal variations and human interventions. The current model does not account for temporal shifts in vegetation and hydrology. Integrating multi-temporal RS data and time-series analysis can enhance the

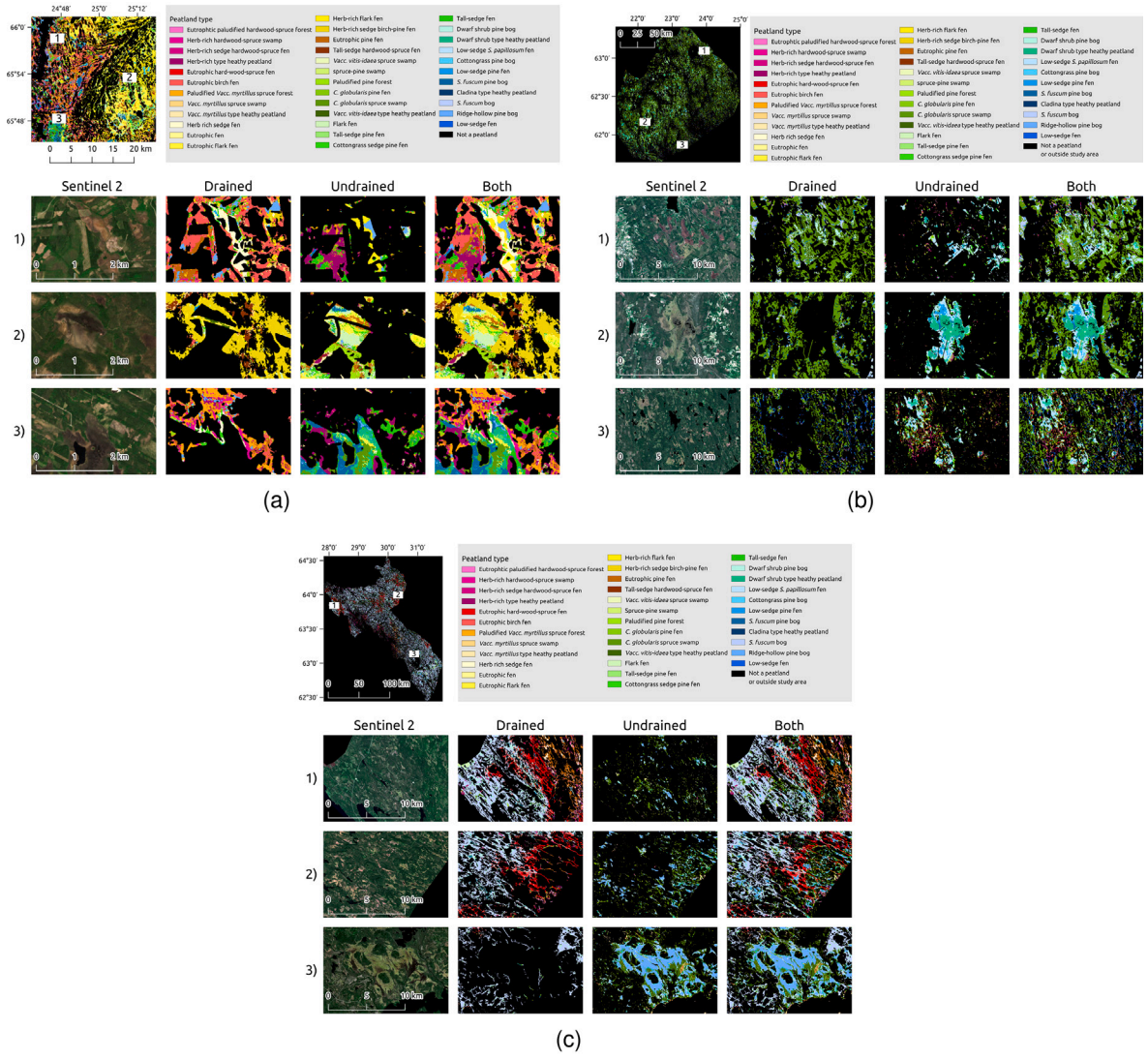

Fig. 7. Prediction map of site types for (a) Kemi, (b) SO and (d) EF. Details of the classification map for three subregions (1–3) can be compared to the true color S2 image.

model's ability to track changes over time and improve classification stability.

- Sensor-Specific Limitations: Certain sensors, such as Sentinel-1, are sensitive to soil moisture but less effective for detailed vegetation classification. Similarly, Sentinel-2 has limitations in penetrating dense canopies. Future extensions of this work will explore the inclusion of L-band SAR and hyperspectral data for deeper canopy penetration and improved spectral resolution.
- Generalization Across Diverse Ecological Zones: While the model demonstrated strong performance in the three study areas in Finland, its generalization capability to other geographic regions with different ecological characteristics is yet to be validated. We plan to extend our study to other boreal and temperate peatlands to evaluate model adaptability.
- Computational Complexity: The multi-stream CNN architecture and sliding-window approach are computationally demanding, especially when processing high-resolution multi-source data. We are exploring model optimization strategies, such as pruning and quantization, to reduce computational load without sacrificing accuracy.

We believe that addressing these limitations will not only improve the classification accuracy but also extend the applicability of the proposed approach for large-scale peatland monitoring and greenhouse gas inventory assessments.

As future work, we intend to explore incorporating additional geospatial data sources, such as thermal imagery, L-band SAR, hyperspectral data, and high-resolution LiDAR, to capture finer spatial and ecological variations. We also have plan to expand the training dataset to improve model stability and generalization A future goal is also to apply the proposed CNN model on a larger training set and harmonized input RS and GIS datasets which would cover the entire country.

6. Conclusion

Peatland habitats are heterogenous, spatially highly variable, and structurally complex. This makes prediction of the exact ecological site type and their fertility levels with RS and GIS data and deep learning a challenging task at national scale. This study demonstrates the effectiveness of integrating diverse geospatial datasets with a well-known DL method (CNN) for mapping a high number of boreal peatland classes. By employing a selective search for feature selection and a sliding window approach, we reduced the computational time and complexities. Regardless of the limitations of the training data, the fertility levels of the site types could be predicted relatively accurately. The classification accuracies for the undrained peatlands were most acceptable, but slightly less so for the drained peatlands. The results

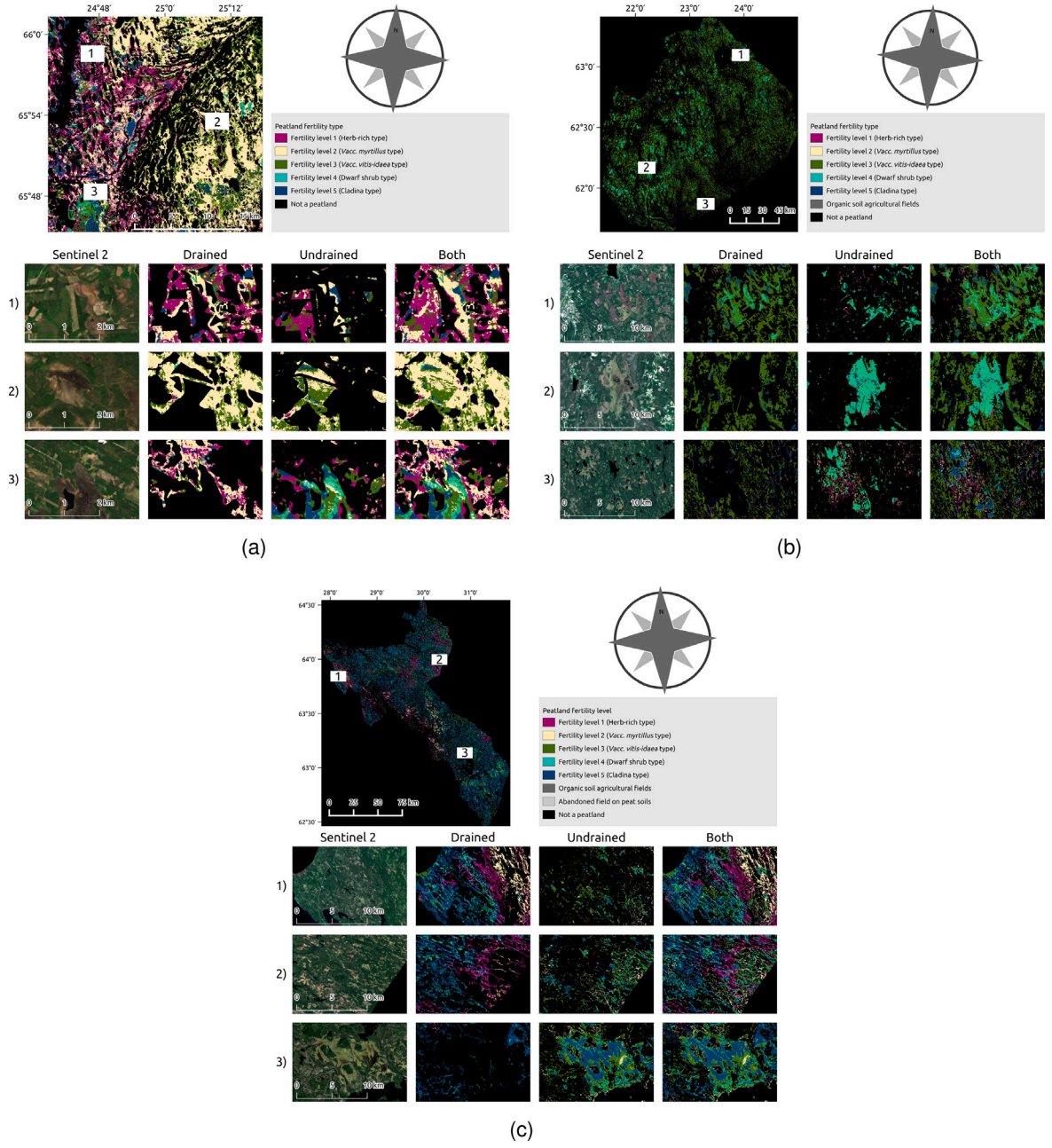

Fig. 8. Prediction map of fertility classes for (a) Kemi, (b) SO and (d) EF. Details of the classification map for three subregions (1–3) can be compared to the true color S2 image.

of the study present the restrictions of the approach in national scale peatland mapping for improving greenhouse gas (GHG) inventories and conservation planning.

CRediT authorship contribution statement

Luca Zelioli: Validation, Software, Methodology, Investigation. **Fahimeh Farahnakian:** Writing – review & editing, Writing – original draft, Visualization, Validation, Supervision, Software, Methodology, Investigation, Conceptualization. **Maarit Middleton:** Writing – review & editing, Methodology, Investigation, Funding acquisition, Formal analysis, Data curation, Conceptualization. **Timo P. Pitkänen:** Writing – review & editing, Visualization, Validation, Formal analysis, Data curation. **Sakari Tuominen:** Visualization, Validation, Supervision, Resources, Formal analysis, Conceptualization. **Paavo Nevalainen:** Writing – review & editing, Validation, Methodology, Investigation. **Jonne Pohjankukka:** Writing – original draft, Validation, Methodology, Investigation, Data curation. **Jukka Heikkonen:** Writing – review & editing, Visualization, Supervision, Resources, Project administration, Formal analysis.

Declaration of competing interest

The authors declare the following financial interests/personal relationships which may be considered as potential competing interests: Fahimeh Farahnakian reports financial support was provided by Ministry of Agriculture and Forestry of Finland. If there are other authors, they declare that they have no known competing financial interests or personal relationships that could have appeared to influence the work reported in this paper.

Acknowledgments

This work is part of the Advances in soil information- MaaTi project funded by the Ministry of Agriculture and Forestry of Finland (2021–2022, funding decision VN/27416/2020-MMM-2). The authors wish to acknowledge CSC – IT Center for Science, Finland, for computational resources, and the MaaTi project management and steering group for constructive comments during the work. The TerraSAR-X and RADARSAT-2 data were supplied through the European Space Agency's Third party mission proposals no. 36096 "Remote sensing as a tool for mapping and evaluating peatlands and peatland carbon stock in Northern Finland; Radarsat-2" and no. 36096 "Remote sensing as a tool for mapping and evaluating peatlands and peatland carbon stock in Northern Finland; Radarsat-2" and by Maarit Middleton in year 2017.

Data availability

Our code and models are available on GitHub at https://github.com/MaaTi-project/Peatland-MultiSensor-CNN. GTK peatland inventory observations, consisting part of the training data used for modeling, is publicly available but subject to a charge (https://tupa.gtk.fi/paikkatieto/meta/turvevarojen_tilinpitotiedot.html). The remaining part of the training data, consisting of Luke NFI observations, is not public and cannot be shared. Most remote sensing data sources are available as open data and free of charge from the following links: https://asiointi.maanmittauslaitos.fi/karttapaikka/tiedostopalvelu?lang=en(DEM), https://www.metsakeskus.fi/fi/avoin-metsa-ja-luontotieto/aineistot-paikkatieto-ohjelmille/paikkatietoaineistot(CHM), and http://kartta.luke.fi/index-en.html (MS-NFI). RadarSAT and TerraSAR-X data are commercial products and available from the data provider for a licensing fee. The processed Sentinel-1 and Sentinel-2 data as well as the LBP rasters derived from DEM and CHM are not available online but may be requested from the authors.

References

Amoakoh, A.O., Aplin, P., Awuah, K.T., Delgado-Fernandez, I., Moses, C., Alonso, C.P., 2021. Tropical peatland classification using multi-sensor sentinel imagery and random forest algorithm in Greater Amanzule, Ghana. In: 2021 IEEE International Geoscience and Remote Sensing Symposium IGARSS. pp. 5910–5913.

Bourgeau-Chavez, L., Sarah, E., Powell, R., Battaglia, M., Benscoter, B., Turetsky, M., Kasischke, E., Banda, E., 2016. Mapping boreal peatland ecosystem types from Multi-Temporal radar and optical satellite imagery. Can. J. Forest Res. 47.

Cajander, A., 1913. Studies about Finnish peatlands. Silva Fenn. 2 (3).

Chasmer, L., Mahoney, C., Millard, K., Nelson, K., Peters, D., Merchant, M., Hopkinson, C., Brisco, B., Niemann, O., Montgomery, J., Devito, K., Cobbaert, D., 2020. Remote Sensing of Boreal Wetlands 2: Methods for evaluating boreal wetland ecosystem state and drivers of change. Remote. Sens. 12 (8), [Online]. Available: https://www.mdpi.com/2072-4292/12/8/1321.

de Bem, P.P., de Carvalho Junior, O.A., Fontes Guimarães, R., Trancoso Gomes, R.A., 2020. Change detection of deforestation in the Brazilian amazon using landsat data and convolutional neural networks. Remote. Sens. 12 (6), [Online]. Available: https://www.mdpi.com/2072-4292/12/6/901.

Dechka, J., Franklin, S., Watmough, M., Bennett, R., Ingstrup, D., 2002. Classification of wetland habitat and vegetation communities using multi-temporal Ikonos imagery in Southern Saskatchewan. Can. J. Remote Sens. 28, 679–685.

2023. erraSAR-X, ground segment, basic product specification document.

Erudel, T., Fabre, S., Briottet, X., Houet, T., 2017. Classification of peatland vegetation types using in situ hyperspectral measurements. In: 2017 IEEE International Geoscience and Remote Sensing Symposium. IGARSS, pp. 5713–5716.

Esmaeili, M., Abbasi-Moghadam, D., Sharifi, A., Tariq, A., Li, Q., 2023. ResMorCNN model: Hyperspectral images classification using residual-injection morphological features and 3DCNN layers. IEEE J. Sel. Top. Appl. Earth Obs. Remote. Sens. 17, 219–243.

Fahimeh, F., Jukka, H., 2020. Deep learning based multi-modal fusion architectures for maritime vessel detection. Remote. Sens. 12 (16), [Online]. Available: https://www.mdpi.com/2072-4292/12/16/2509.

Farahnakian, F., Haghbayan, M.-H., Poikonen, J., Laurinen, M., Nevalainen, P., Heikkonen, J., 2018. Object detection based on multi-sensor proposal fusion in maritime environment. In: 2018 17th IEEE International Conference on Machine Learning and Applications. ICMLA, pp. 971–976.

Farahnakian, F., Heikkonen, J., 2020. A comparative study of deep learning-based RGB-depth fusion methods for object detection. In: 2020 19th IEEE International Conference on Machine Learning and Applications. ICMLA, pp. 1475–1482.

Farahnakian, F., Zelioli, L., Middleton, M., Seppä, I., Pitkänen, T., Heikkonen, J., 2023a. CNN-based boreal peatland fertility classification from sentinel-1 and sentinel-2 imagery. In: 2023 IEEE International Symposium on Robotic and Sensors Environments. ROSE, Tokyo, Japan, pp. 1–7.

Farahnakian, F., Zelioli, L., Pitkänen, T., Pohjankukka, J., Middleton, M., Tuominen, S., Nevalainen, P., Heikkonen, J., 2023b. Multistream convolutional neural network fusion for Pixel-wise classification of Peatland. In: 2023 26th International Conference on Information Fusion. FUSION, pp. 1–8.

Farmonov, N., Esmaeili, M., Abbasi-Moghadam, D., Sharifi, A., Amankulova, K., Mucsi, L., 2024. HypsLiDNet: 3D-2D CNN model and spatial–spectral morphological attention for crop classification with DESIS and LiDAR data. IEEE J. Sel. Top. Appl. Earth Obs. Remote. Sens. 17, 1–34.

Finland, S., 2022. Greenhouse Gas Emissions in Finland 1990 to 2020. National Inventory Report under the UNFCCC and the Kyoto Protocol.

Ghobadi, Y., Pradhan, B., Kabiri, K., Pirasteh, S., Shafri, H.Z.M., Sayyad, G.A., 2012. Use of multi-temporal remote sensing data and GIS for wetland change monitoring and degradation. In: 2012 IEEE Colloquium on Humanities, Science and Engineering. CHUSER, pp. 103–108.

Harris, A., Bryant, R., Baird, A., 2006. Mapping the effects of water stress on Sphagnum: Preliminary observations using airborne remote sensing. Remote Sens. Environ. 100 (3), 363–378, [Online]. Available: https://www.sciencedirect.com/science/article/pii/S0034425705003809.

Henderson, F.M., Lewis, A.J., 2008. Radar detection of wetland ecosystems: a review. Int. J. Remote Sens. 29 (20), 5809–5835, [Online]. Available: https://doi.org/10.1080/01431160801958405.

Hodgson, M.E., 1998. What size window for image classification? A cognitive perspective. Photogramm. Eng. Remote Sens. 64, 797–807.

Ioffe, S., Szegedy, C., 2015. Batch normalization: Accelerating deep network training by reducing Internal Covariate Shift. CoRR, abs/1502.03167 [Online]. Available: http://arxiv.org/abs/1502.03167.

Jamali, A., Mahdianpari, M., Mohammadimanesh, F., Brisco, B., Salehi, B., 2021. A synergic use of sentinel-1 and sentinel-2 imagery for complex wetland classification using generative adversarial network (GAN) scheme. Water 13 (24), 3601.

Kampffmeyer, M., Salberg, A.-B., Jenssen, R., 2016. Semantic segmentation of small objects and modeling of uncertainty in urban remote sensing images using deep convolutional neural networks. In: 2016 IEEE Conference on Computer Vision and Pattern Recognition Workshops. CVPRW, pp. 680–688.

Korpela, I., Koskinen, M., Vasander, H., Holopainen, M., Minkkinen, K., 2009. Airborne small-footprint discrete-return LiDAR data in the assessment of boreal mire surface patterns, vegetation and habitats. Forest Ecol. Manag. 258 (7), 1549–1566.

Krizhevsky, A., Sutskever, I., Hinton, G.E., 2012a. ImageNet classification with deep convolutional neural networks. In: Pereira, F., Burges, C., Bottou, L., Weinberger, K. (Eds.), Advances in Neural Information Processing Systems. Vol. 25, Curran Associates, Inc., [Online]. Available: https://proceedings.neurips.cc/paper/2012/file/c399862d3b9d6b76c8436e924a68c45b-Paper.pdf.

Krizhevsky, A., Sutskever, I., Hinton, G.E., 2012b. ImageNet classification with deep convolutional neural networks. In: Pereira, F., Burges, C., Bottou, L., Weinberger, K. (Eds.), Advances in Neural Information Processing Systems. Vol. 25, Curran Associates, Inc., [Online]. Available: https://proceedings.neurips.cc/paper_files/paper/2012/file/c399862d3b9d6b76c8436e924a68c45b-Paper.pdf.

Laine, J., Vasander, H., Hotanen, J.-P., Nousiainen, H., Saarinen, M., Penttilä, T., 2018. Key to Finnish mire types. p. 1602.

Li, W., Chen, C., Zhang, M., Li, H., Du, Q., 2019. Data augmentation for hyperspectral image classification with deep CNN. IEEE Geosci. Remote. Sens. Lett. 16 (4), 593–597.

Li, Y., Zhang, H., Xue, X., Jiang, Y., Shen, Q., 2018. Deep learning for remote sensing image classification: A survey. Wiley Interdiscip. Rev.: Data Min. Knowl. Discov. 8, e1264.

Liao, C., Wang, J., Xie, Q., Baz, A.A., Huang, X., Shang, J., He, Y., 2020. Synergistic use of multi-temporal RADARSAT-2 and VENμS data for crop classification based on 1D convolutional neural network. Remote. Sens. 12 (5), [Online]. Available: https://www.mdpi.com/2072-4292/12/5/832.

Ltd, M.T., 2018. RADARSAT-2 Product description.

Mahdianpari, M., Salehi, B., Rezaee, M., Mohammadimanesh, F., Zhang, Y., 2018. Very deep convolutional neural networks for complex land cover mapping using multispectral remote sensing imagery. Remote. Sens. 10 (7), 1119.

Mäkisara, K., Katila, M., Peräsaari, J., 2022. The multi-source national forest inventory of Finland — methods and results 2017 and 2019. In: Natural Resources and Bioeconomy Studies 90/2022. Natural Resources Institute Finland, p. 73.

Marcano-Cedeño, A., Quintanilla-Domínguez, J., Cortina-Januchs, M.G., Andina, D., 2010. Feature selection using sequential forward selection and classification applying artificial metaplasticity neural network. In: IECON 2010 - 36th Annual Conference on IEEE Industrial Electronics Society. pp. 2845–2850.

Merchant, M.A., Adams, J.R., Berg, A.A., Baltzer, J.L., Quinton, W.L., Chasmer, L.E., 2017. Contributions of C-band SAR data and polarimetric decompositions to subarctic boreal peatland mapping. IEEE J. Sel. Top. Appl. Earth Obs. Remote. Sens. 10 (4), 1467–1482.

Middleton, M., Laatikainen, M., Kivilompolo, J., Harju, A., Lerssi, J., Valkama, M., Pitkänen, T., Pohjankukka, J., Balazs, A., Tuominen, S., Zelioli, L., Farahnakian, F., Nevalainen, P., Heikkonen, J., 2023. Technical Description for the Peatland Site Type Data of Finland. Tech. Rep., Geological Survey of Finland (GTK).

Middleton, M., Närhi, P., Arkimaa, H., Hyvönen, E., Kuosmanen, V., Treitz, P., Sutinen, R., 2012. Ordination and hyperspectral remote sensing approach to classify peatland biotopes along soil moisture and fertility gradients. Remote Sens. Environ. 124, 596–609, [Online]. Available: https://www.sciencedirect.com/science/article/pii/S0034425712002465.

Millard, K., Richardson, M., 2015. On the importance of training data sample selection in random forest image classification: A case study in Peatland Ecosystem Mapping. Remote. Sens. 7 (7), 8489–8515, [Online]. Available: https://www.mdpi.com/2072-4292/7/7/8489.

Mohammad, E., Abbasi-Moghadam, D., Sharifi, A., Tariq, A., Li, Q., 2023. Hyperspectral image band selection based on CNN embedded GA (CNNeGA). IEEE J. Sel. Top. Appl. Earth Obs. Remote. Sens. 16, 1927–1950.

Mohammadimanesh, F., Salehi, B., Mahdianpari, M., Brisco, B., Gill, E., 2019. Full and simulated compact polarimetry SAR responses to Canadian wetlands: Separability analysis and classification. Remote. Sens. 11 (5), 516.

of Finland (NLS), N.L.S., 2023. Elevation model 2 m.

Päivänen, J., Hånell, B., 2012. Peatland ecology and forestry: A sound approach. In: Helsingin yliopiston metsätieteiden laitoksen julkaisuja, Department of Forest Ecology, University of Helsinki, [Online]. Available: https://books.google.fi/books?id=1b9QmwEACAAJ.

Pang, Y., Räsänen, A., Juselius-Rajamäki, T., Aurela, M., Juutinen, S., Väliranta, M., and, T.V., 2023. Upscaling field-measured seasonal ground vegetation patterns with sentinel-2 images in boreal ecosystems. Int. J. Remote Sens. 44 (14), 4239–4261, [Online]. Available: https://doi.org/10.1080/01431161.2023.2234093.

Peltoniemi, J.I., Kaasalainen, S., Näränen, J., Rautiainen, M., Stenberg, P., Smolander, H., Smolander, S., Voipio, P., 2005. BRDF measurement of understory vegetation in pine forests: dwarf shrubs, lichen, and moss. Remote Sens. Environ. 94 (3), 343–354, [Online]. Available: https://www.sciencedirect.com/science/article/pii/S0034425704003311.

Pietikäinen, M., Hadid, A., Zhao, G., Ahonen, T., 2011. Computer Vision Using Local Binary Patterns, first ed. Springer Publishing Company, Incorporated.

Pouliot, D., Latifovic, R., Pasher, J., Duffe, J., 2019. Assessment of convolution neural networks for wetland mapping with landsat in the central Canadian Boreal Forest Region. Remote. Sens. 11 (7), [Online]. Available: https://www.mdpi.com/2072-4292/11/7/772.

Programme, U.N.E., 2022-11. Global peatlands assessment: The state of the world's peatlands - Evidence for action toward the conservation, restoration, and sustainable management of peatlands - summary for policy makers. [Online]. Available: https://wedocs.unep.org/20.500.11822/41236.

Räsänen, A., Aurela, M., Juutinen, S., Kumpula, T., Lohila, A., Penttilä, T., Virtanen, T., 2020. Detecting northern peatland vegetation patterns at ultra-high spatial resolution. Remote. Sens. Ecol. Conserv. 6 (4), 457–471.

Räsänen, A., Virtanen, T., 2019. Data and resolution requirements in mapping vegetation in spatially heterogeneous landscapes. Remote Sens. Environ. 230.

resources institute Finland (LUKE), N., 2021. Advances in soil information.

Rezaee, M., Mahdianpari, M., Zhang, Y., Salehi, B., 2018a. Deep convolutional neural network for complex wetland classification using optical remote sensing imagery. IEEE J. Sel. Top. Appl. Earth Obs. Remote. Sens. 11 (9), 3030–3039.

Rezaee, M., Mahdianpari, M., Zhang, Y., Salehi, B., 2018b. Deep convolutional neural network for complex wetland classification using optical remote sensing imagery. IEEE J. Sel. Top. Appl. Earth Obs. Remote. Sens. 11 (9), 3030–3039.

Rudner, T., Rußwurm, M., Fil, J., Pelich, R., Bischke, B., Kopackova-Strnadova, V., Biliński, P., 2019. Multi3Net: Segmenting flooded buildings via fusion of multiresolution, multisensor, and multitemporal satellite imagery. Proc. AAAI Conf. Artif. Intell. 33, 702–709.

Sharifi, A., Esmaeili, M., Abbasi-Moghadam, D., Tariq, A., Li, Q., 2025. Multimodal deep learning for hyperspectral and LiDAR data fusion in land cover classification. IEEE J. Sel. Top. Appl. Earth Obs. Remote. Sens. 18, 1–15.

Sharifi, A., Safari, M., 2025. Enhancing the spatial resolution of sentinel-2 images through super-resolution using transformer-based deep learning models. IEEE J. Sel. Top. Appl. Earth Obs. Remote. Sens. PP, 1–17.

Sugumaran, R., Harken, J., Gerjevic, J., 2004. Using remote sensing data to study wetland dynamics in Iowa.

Touzi, R., Gosselin, G., Brooks, R., 2019. Polarimetric L-band SAR for peatland mapping and monitoring, "ESA Book on principles and applications of Pol-InSAR. in press.

2022. Tuotekuvaus: Latvusmallit. Electronic resource.

Ustin, S.L., Gitelson, A., Jacquemoud, S., Schaepman, M., Asner, G.P., Gamon, J.A., Zarco-Tejada, P., 2009. Retrieval of foliar information about plant pigment systems from high resolution spectroscopy. Remote Sens. Environ. 113, S67–S77, [Online]. Available: https://www.sciencedirect.com/science/article/pii/S0034425709000789, Imaging Spectroscopy Special Issue.

Virtanen, K., 2020. Geologian tutkimuskeskuksen turvetiedonkeruun suotyyppiopas. 2017. abstract: Peatland site types guide book in gtk. Turvetutkimusraportti 467. peatland study raport 467. Geological survey of Finland..

Zeng, X., Martinez, T., 2001. Distribution-balanced stratified cross-validation for accuracy estimation. J. Exp. Theor. Artif. Intell. 12.